

A Novel Bifunctional Nanoplatfom with Aggregation-Induced Emission Property for Efficient Photodynamic Killing of Bacteria and Wound Healing

Biao Hou^{1,*}, Fen Yang^{2,*}, Chaotao Hu¹, Changxiong Liu¹, Xiangjun Xiao¹, Yanming Chen¹, Xiongjie Huang¹, Songlin Xie¹

¹Department of Hand and Foot Microsurgery, The Affiliated Nanhua Hospital, Hengyang Medical College, University of South China, Hengyang, People's Republic of China; ²Department of Infectious Diseases, The Affiliated Nanhua Hospital, Hengyang Medical College, University of South China, Hengyang, People's Republic of China

*These authors contributed equally to this work

Correspondence: Songlin Xie, Department of Hand and Foot Microsurgery, The Affiliated Nanhua Hospital, Hengyang Medical College, University of South China, No. 336 Dongfeng Nan Road, Zhuhui District, Hengyang, 421002, People's Republic of China, Tel + 86- 139- 7540- 4959, Email xiesonglin0929@163.com

Background: Photodynamic antimicrobial therapy (PDAT) has been extensively studied because of its potential applications such as precise controllability, high spatiotemporal accuracy, and non-invasiveness. More importantly, it is difficult for bacteria to develop resistance to the aforementioned PDATs. However, the selectivity of traditional PDAT methods to bacteria is generally poor, so it has been proposed to introduce positively charged components such as quaternary ammonium salts to enhance the targeting of bacteria; however, they always possess high toxicity to normal cells. As a result, measures should be taken to enhance the targeting of bacteria and avoid side effects on normal cells.

Methods and Results: In our work, we creatively design a nanoplatfom with high anti-bacterial efficiency, low side effects and its size is approximately 121 nm. BSA, as a nanocarrier, encapsulates the photosensitizer (E)-4-(4-(diphenylamino)styryl)-1-methylpyridin-1-ium with AIE properties named as BSA-Tpy, which increases its circulation time in vivo and improves the biocompatibility. Under acidic conditions (pH = 5.0), the surface positive charge of the BSA-Tpy is increased to +18.8 mV due to protonation of amine residues to achieve the targeting effect on bacteria. Besides, under the irradiation of white light, the BSA-Tpy will produce ROS to kill bacteria efficiently about 99.99% for both Gram-positive and Gram-negative bacteria, which shows the potential application value for the treatment of infected wounds.

Conclusion: We have developed a feasible method for photodynamic antibacterial therapy, possessing excellent biocompatibility and high antibacterial efficiency with good fluorescence imaging property.

Keywords: bovine serum albumin nanocarriers, aggregate induced emission, photodynamic antibacterial therapy, antimicrobial resistance

Introduction

The high level of antibiotic resistance of pathogenic bacteria has become a major problem for health care.^{1,2} Therefore, it is imperative to propose efficient and non-resistance-inducing antibacterial methods. Photodynamic antimicrobial therapy (PDAT) is the essential choice for the treatment of pathogenic bacteria, which mainly includes three factors: light irradiation, photosensitizers and molecular oxygen.³⁻⁵ Briefly, the photosensitizer (PS) is excited from the ground state to the excited state at the appropriate light wave, and then interacts with oxygen to produce singlet oxygen and reactive oxygen species (ROS), causing oxidative damage to target bacteria.⁶⁻⁸ More importantly, in the PDAT process, the photosensitizer does not

need to penetrate the interior of the bacteria, and the generated reactive oxygen species destroy the external structure of the bacteria, resulting in the leakage of internal components, which make it difficult to develop drug resistance.^{9,10}

However, traditional photosensitizers usually suffer from small Stokes shifts, poor chemical stability, limited fluorescence imaging capabilities, and low ROS yields.^{11–13} Unfortunately, some photosensitizers suppress the emission in the aggregated state due to the π - π stacking effect of aromatic hydrocarbons and their derivatives, resulting in poor imaging ability and low ROS yield. So far, advanced plasmas with aggregation-induced emission (AIE) characteristics have been developed. This structural feature enables them to emit light with high efficiency in the aggregated state due to the restriction of free rotation within the molecule. Furthermore, photosensitizers with AIE properties can efficiently generate ROS in the aggregated state, providing high-performance effects during treatment. Furthermore, the efficiency of PS to generate ROS is highly dependent on intersystem crossing (ISC).^{14–16} The scientists found that through the HOMO-LUMO design of the D- π -A structure, the ISC can be tuned such that the energy gap between the triplet state (T1) and the singlet state (S1) is small.^{17–20}

Unfortunately, molecular photosensitizers are often unstable and hydrophobic in aqueous solution, which may limit their applications.^{21,22} To address these issues, various nanoparticle platforms have been developed, such as liposomes, silica, metals, and bovine serum albumin nanoparticles.^{23,24} Among them, bovine serum albumin nanocarriers have attracted more and more interest than other nanomaterials due to their wide range of applications. On the one hand, the hydrophilic outer part of the nanoparticles has excellent water solubility, which can prolong the circulation time in vivo; on the other hand, the hydrophobic inner core tends to aggregate, which is beneficial to the above-mentioned photosensitizers with AIE properties. As an endogenous substance, bovine serum albumin (BSA) has good compatibility, non-toxicity, no antigenicity, safe metabolites, and no autoimmune reaction. At the same time, it possesses great stability at a certain temperature and pH compared to other nanomaterials.^{25–28} So far, poor bacterial selectivity of the reported PDAT method is still a problem remained that may inevitably lead to off target toxicity and low efficiency. In order to furtherly improve the targeting effect, biological stimuli system has been investigated in response to biological stimuli, such as pH, redox potential, and dysregulated enzymes. It is worth noting that the infected tissues are characterized by low pH value due to the accumulation of lactic and acetic acids as a result of low oxygen-triggered anaerobic fermentation. As a result, pH-responsive system was proven to be a feasible strategy, which may improve therapeutic bacteria-targeting effect. Under acidic conditions, the nanoparticle surface charge is converted to a positive charge due to protonation of amine residues. Besides, the unique spatial structure of albumin can encapsulate drugs through physical entrapment or chemical bonding. For most exogenous drugs, albumin can improve the stability by encapsulating it as well as improving drug loading performance.^{29,30}

Inspired by the advanced research, in this contribution, we fabricated a novel system named BSA-Tpy which has high biocompatibility and high antibacterial efficiency for the purpose of applying in the repair of bacterial infection wound. Under acidic conditions, the nanoparticle surface charge is converted to a positive charge due to protonation of amine residues.

Materials and Methods

Materials

Dimethyl sulfoxide (DMSO), petroleum ether, ethyl acetate and anhydrous ether were obtained from Aladdin. Methicillin-resistant *Staphylococcus aureus* (MRSA) and *E. coli* were isolated from human clinical specimens, and identified in the Clinical Microbiology Laboratory, The affiliated Nanhua Hospital, Hengyang Medical College, University of South China (Hengyang, China). NIH/3T3 cell lines were kindly provided by Dr. Chaotao Hu (The affiliated Nanhua Hospital). 4-methylpyridine, 2,2'-4-(diphenylamino)benzaldehyde were purchased from Tansoole. These other used solvents and reagents were of analytical purity and were purchased from commercial sources. Deionized water was used during the process.

Characterization

The size distribution and the zeta potential of the BSA-Tpy in PBS were measured by Zetasizer Nano S90. The absorbance of the cells was detected by a microplate reader (Thermo Varioskan Flash, USA). The fluorescence was measured using an F-7000 fluorospectrophotometer (HITACHI, Japan). The bacterial morphology was recorded using Inspect F scanning electron

microscope (Philips, Netherlands). The Laser scanning confocal microscope was used to record the fluorescence images. The morphology of material detected with a transmission electron microscope (JEOL, Japan).

Synthesis of Photosensitizer

In brief, 4-(diphenylamino)benzaldehyde and 4-methylpyridine were dissolved in DMSO followed by stirring at 85 °C overnight. Next, it was cooled to room temperature followed by precipitating into anhydrous ether to obtain pink solid (Figure S1). Finally, it was re-dissolved with KPF6 solution (3 mL) for 3h and then evaporated by compressed air.

Preparation and Characterization of BSA-Tpy NPs

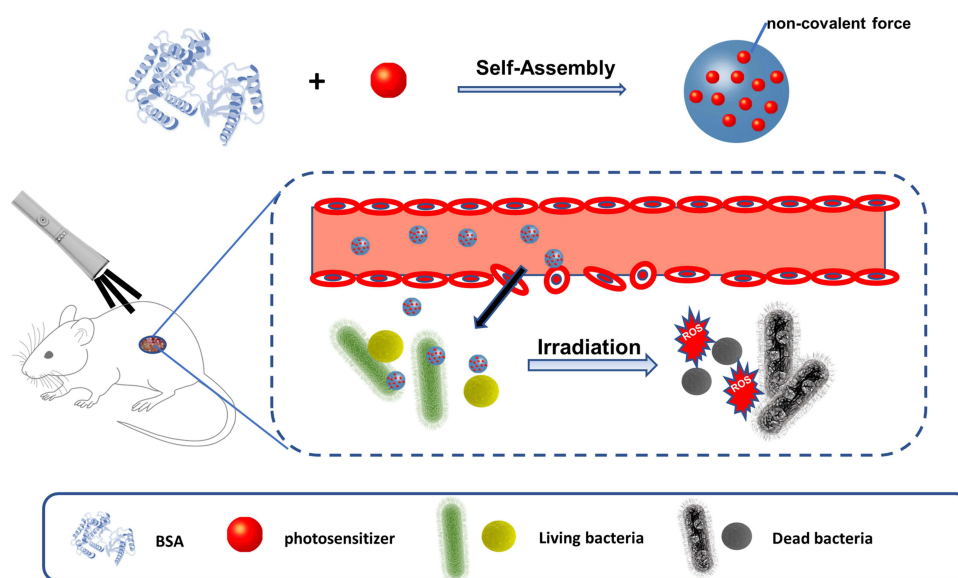
As shown in Scheme 1, typically, BSA-Tpy NPs were prepared by the desolubilization method. Briefly, a certain amount of BSA was dissolved in ionized water (50 mg/mL). After 30 minutes, under stirring at a rotational speed of 800 rpm at room temperature, and then ethanol dissolved with 10 mg photosensitizer was continuously added to the solution. After 1 hour stirring, 40 μ L of 2% glutaraldehyde was added to the system to obtain stable BSA-Tpy NPs. The resulting suspension was stirred overnight at room temperature in the dark. Finally, NP particles were obtained after centrifugation three times at 20,000 g for 30 minutes at 4 °C. NP pellets were resuspended in either 5% glucose. Finally, the BSA-Tpy NPs were stored in a sterile environment to facilitate further operation. Its hydrodynamic diameters, PDI was regarded as the index of evaluating its stability. An average value of three repeated measurements at room temperature for each sample. Then, TEM. Spectrofluorometer was used to evaluate the morphology of BSA-Tpy NPs.

ROS Measurements Under Irradiation

The method to detect ROS followed by the previous report. Briefly, fresh DCFH was prepared by hydrolysis of DCFH-DA in sodium hydroxide aqueous solution at ambient temperature. The DCFH solution was mixed with BSA-Tpy NPs solution at room temperature. At different time intervals, fluorescence emission intensity was collected under 488 nm excitation wavelength. The DCFH solution without BSA-Tpy NPs and BSA-Tpy NPs without DCFH were set as control groups.

Cell Viability via MTT Assay

Cell viability was assessed with fibroblasts. Briefly, cells were seeded in 96-well plates at a density of 10,000 cells per well and incubated in Dulbecco's Modified Eagle Medium (DMEM) containing 10% fetal bovine serum for 24 h under typical conditions, and then remove the medium. Subsequently, cells were incubated with different concentrations of



Scheme 1 Illustration of BSA-Tpy NPs as a nanoplatform for photodynamic antibacterial therapy.

samples for 30 min, and then incubated under light of $50 \text{ mW}\cdot\text{cm}^{-2}$ for different times. Cells treated with BSA-Tpy NPs and cells untreated with BSA-Tpy NPs were used as negative controls. The cells were cultured 24 h after the new medium was replaced. After removing the cell culture medium, add 100 μL of fresh culture medium to each well. After incubation for 3 h, the MTT solution was removed and 100 μL of DMSO was added to each well. The absorbance at 490 nm was recorded with a microplate reader. The formula for calculating relative cell viability is as follows:

$$\text{Cell viability(\%)} = (A1 - A0) / (A_{\text{control}} - A0) \times 100\%$$

A0, A1 and Acontrol represented the absorbance of samples, the absorbance of cells and the absorbance of MTT assay without samples.

Bacterial Culturing and Staining of BSA-Tpy NPs

The method to culture and stain bacteria with BSA-Tpy NPs was followed according to the previous research. In brief, bacteria were put into 10 mL medium, incubating for half of day. Afterwards, the concentrations of bacteria were calculated by measuring optical density at 600 nm, followed by moving to a 2.0 mL centrifuge tube. Bacteria were harvested by centrifuging at 7500 rpm for 10 min. Then, put 1 mL of BSA-Tpy NPs solution into the centrifuge tube, respectively, after removing the supernatant. The final concentration of NPs is 50 $\mu\text{g}/\text{mL}$ and then incubated together at room temperature, and finally, 5 μL of stained bacteria solution was transferred to glass slide to obtain the samples. These bacteria were imaged by the CLSM.

Photodynamic Antibacterial Experiments

Bacterial suspensions ($\text{OD}_{600} = 10^9 \text{ CFU}/\text{mL}$) were mixed with BSA-Tpy NPs (50 $\mu\text{g}/\text{mL}$) solution, then irradiating under light with different time intervals. At the same time, the bacteria without NPs in PBS at pH 5.0 and pH 7.4 were set as control groups. Then, the bacterial mixtures were diluted to 1×10^5 fold and coated on the solid LB agar plate, afterwards, culturing at 37 $^{\circ}\text{C}$ for 24 h. Antibacterial effect was evaluated by plate counting method. The mentioned experiment was done in parallel three times.

Morphology Studies

Scanning electron microscopy (SEM) was used to evaluate the effect of BSA-Tpy NPs after photodynamic antibacterial experiment. At first, the bacteria were centrifuged and then co-incubated with 2.5% glutaraldehyde solution. After centrifugation, it was incubated with 2.5% glutaraldehyde in PBS. The supernatant was removed and rinsed 3 times with sterile water. Finally, drop the bacterial suspension on a clean silicon wafer in a dry environment at room temperature. All SEM samples were coated with Cu prior to SEM observation and all SEM samples were run in high vacuum mode.

Animal Surgery and Histological Analysis

Normal 8–10 week-male Wistar rats were anesthetized by intraperitoneal injection of 4% sodium pentobarbital. Then, open excision wounds of 1 cm in diameter were made for each rat by excising the dorsal lateral skin on both sides of the spine. The rats were inoculated with *Staphylococcus aureus* suspension ($2 \times 10^8 \text{ CFU}/\text{mL}$) to establish a bacterial infection wound model. Cover all groups with sterile non-woven fabric after treatment. The wound area was photographed with a video camera on the day, day 4 and day 7 post-infection for each. The hearts, livers, spleens, lungs, and kidneys of rats after curing with BSA-Tpy were fixed in 4% paraformaldehyde for histological analysis, then embedded in paraffin, and the fixed tissues were cut into slices with a thickness of 4 mm. H&E stained.

Results and Discussion

Preparation and Characterization of BSA-Tpy NPs

BSA-Tpy NPs were generated by adding ethanol, induced BSA self-assembly into NPs, and then cross-linked BSA molecules with glutaraldehyde to form stable nanoparticles. BSA-Tpy NPs were characterized by dynamic nanolight scattering (DLS), showing diameters of approximately 121 nm (Figure 1A) and the PDI of the nanoparticles is 0.18. Transmission electron microscopy (TEM) revealed spherical NPs (Figure 1B). On the account of existence of both hydrophilic and hydrophobic chain segments, the material could be self-assembled into NPs. The particle size of BSA-Tpy NPs were monitored for days and show no obvious fluctuation (Figure 1B). In addition, it was observed that BSA-Tpy NPs have a good size distribution in PBS, DMEM and

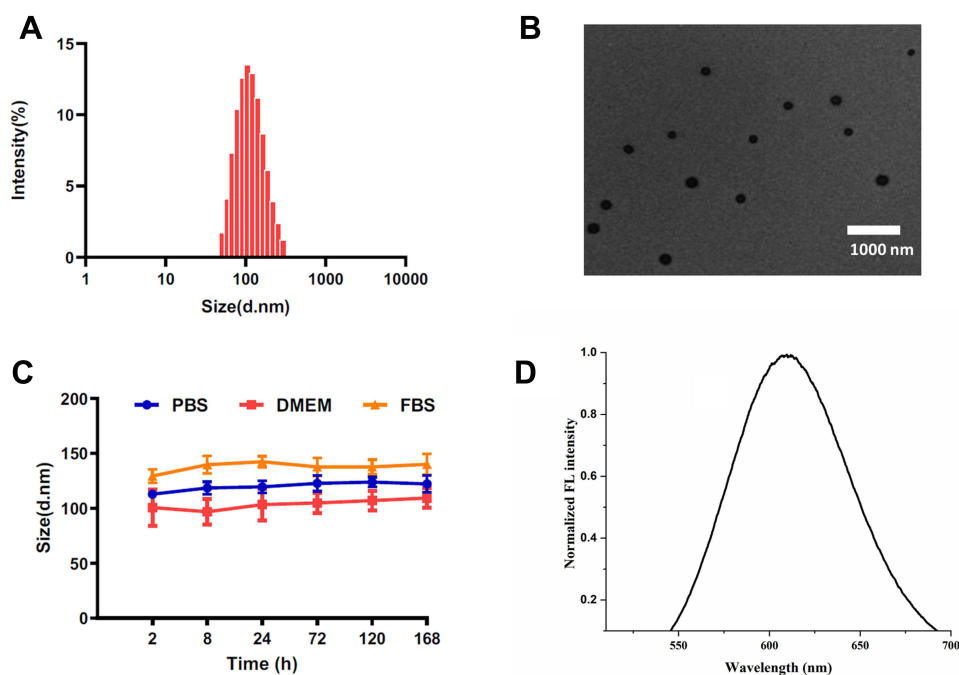


Figure 1 Characterizations of the BSA-Tpy. **(A)** Size distribution of NPs in the water. **(B)** TEM image. **(C)** The stability of BSA-Tpy. **(D)** Normalized FL intensity in water.

10% FBS, proving good colloidal stability. The diameter shown in TEM measurement is slightly smaller because the sample was dried on the copper sheet and the size may narrow down (Figure 1C). In Figure 1D, the normalized fluorescence intensity of the BSA-Tpy NPs was clearly when the water ratio was about 95%, confirming the AIE property. Besides, the emission of BSA-Tpy is about 615 nm due to the strong D- π -A effect leads to the highest occupied molecular orbital (HOMO) and the lowest unoccupied molecular orbital separation (LUMO), proving the potential application in antibacterial field. Then we evaluated the pH-responsive behaviour of the BSA-Tpy NPs. As we have known that the physiological pH in normal tissues and blood is approximately 7.4, but the infected tissues are acidic with low pH values as far as pH 5.0 due to the accumulation of lactic and acetic acids and the low oxygen-triggered anaerobic fermentation. As a result, we tested the behaviour of BSA and BSA-Tpy NPs in response to different pH conditions respectively. As shown in Figure S2, the zeta potential of BSA and BSA-Tpy was -2.4 mV and $+4.9$ mV, respectively, at pH 7.4. Then, they sharply increased to $+8.9$ mV and $+18.8$ mV. We analyzed the possible reasons that under acidic conditions, the nanoparticle surface charge of BSA is converted to a positive charge due to protonation of amine residues.³¹ The results directly proved that the positively charged increased significantly under acidic conditions due to the protonation effect. Hence, this difference between the normal and infected microenvironment endows a great potential for specific targeting of bacteria at infection sites. Besides, the photosensitizer has a characteristic UV absorption peak near 475 nm. The drug loading rate is 17.66% and can be obtained by comparing the absorbance of BSA-Tpy with the standard curve made by the concentration.

ROS Studies

ROS Generation studies of BSA-Tpy NPs. The mechanism of reactive oxygen species produced by materials under light is shown in Figure 2A, from which we can see that intersystem crossing (ISC) is a very important process. The smaller energy of ISC contribute to producing more reactive oxygen species. It has a strong D- π -A effect, which means that it has great potential for long-wavelength emission because long-wavelength emission has the ability to enter deeper tissues as well as reducing cytotoxicity to mammals by light irradiation sources, so it has very ideal biological applications. At the same time, the highest occupied molecular orbital (HOMO) and the lowest unoccupied molecular orbital separation (LUMO) were optimized by the strong D- π -A effect, which reduce the single-triplet energy gap. As a result, it enhanced the production efficiency of amounts of ROS, thereby promoting the application of PDAT.³² Because of the distorted conformation of the triphenylamine (TPA) segment of Tpy in NPs, these compounds have an extended intermolecular distance, which can reduce

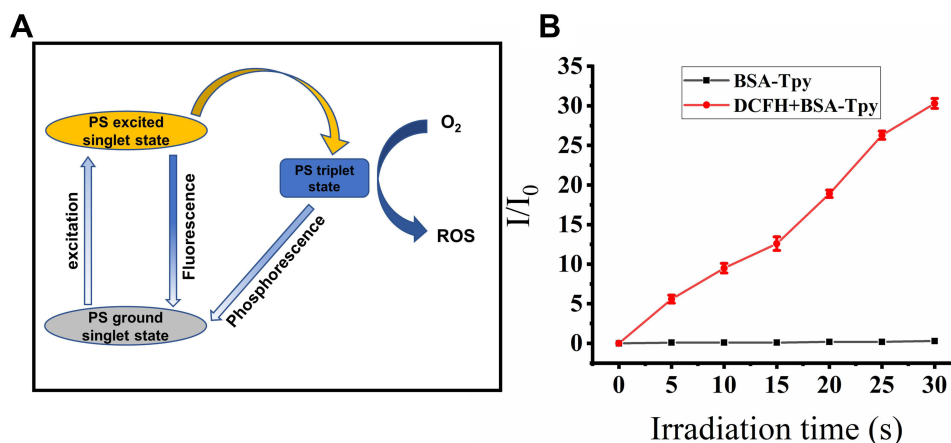


Figure 2 (A) The process and mechanism of ROS produced by materials under light irradiation. **(B)** Plotting of relative PL intensity (I/I_0) at 525 nm versus the irradiation time.

the accumulation of intermolecular π - π , and ultimately inhibit fluorescence quenching during the process to improve the efficiency of reactive oxygen species production.³² Dichlorofluorescein diacetate (DCF-DA) was selected as a probe to detect ROS. As depicted in **Figure 2B**, the intensity of fluorescence gradually increased with the increase of irradiation time. It was clear that the fluorescence intensity increased about 30 times within 30s, proving the production of large amounts of ROS.

In vitro Biocompatibility

Considering the feasibility in practical application, cytotoxicity was measured to evaluate the biocompatibility of the BSA-Tpy NPs. Herein, NIH/3T3 cells were employed in the experiment. As depicted in **Figure 3**, the relative toxicity of

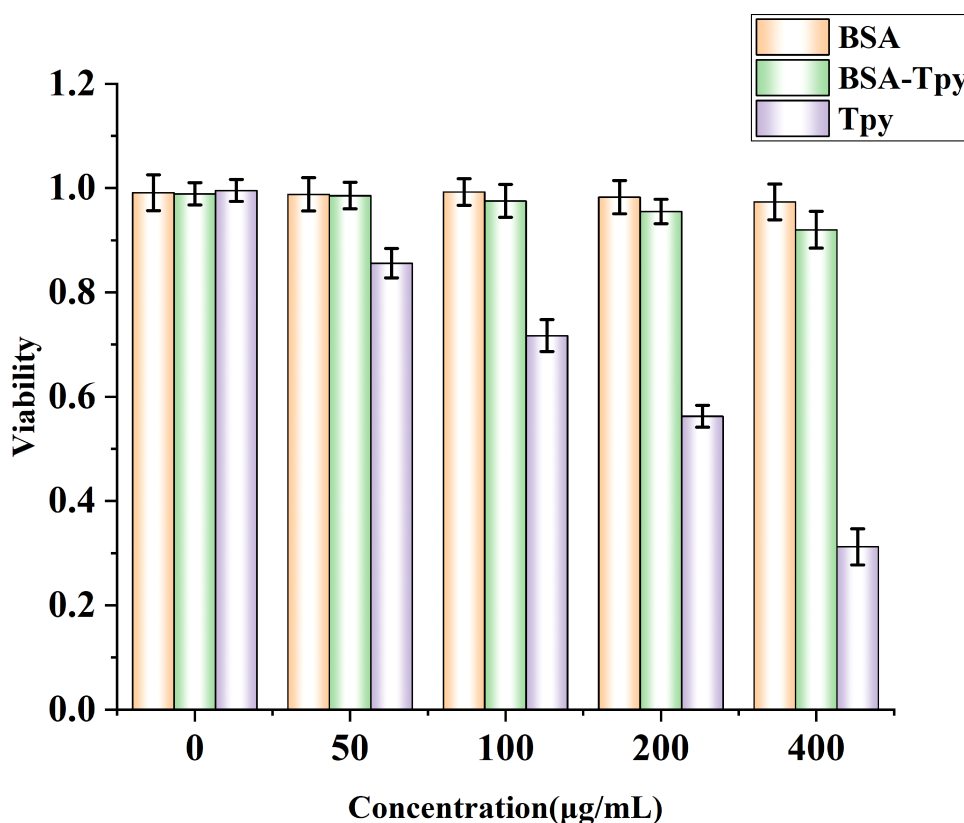


Figure 3 Cell viability of NIH/3T3 cell after being incubated with various concentrations of BSA, BSA-Tpy and Tpy for 24 h in the dark.

Tpy, BSA and BSA-Tpy to normal tissue cells was determined by the MTT Assay. It can be seen from Figure 3 that Tpy alone has a certain degree of cytotoxicity, and the toxicity increases with the increase of the concentration. However, the viability of BSA and BSA-Tpy treated cell maintains a high level of more than 90% at different concentrations. It can be concluded that in the presence of BSA carrier, the toxicity of Tpy toward to normal cells is significantly suppressed, indicating that the cell activity is not affected by the material, proving that the material has high biocompatibility and has the potential for further clinical treatment. When the concentration of the BSA-Tpy is 400 $\mu\text{g/mL}$ the cell ability was still above 90%, indicating excellent biocompatibility in vitro. It achieved the initial design expectation that we introduced BSA into nanopatform to improve the biocompatibility because the BSA would hydrolyse under normal physiological environment (pH 7.4), hiding the positively charged effect of the photosensitizer itself, thus reducing the adsorption between the drug and normal cells. Therefore, the results confirmed the feasibility in practical application.

Photodynamic Antibacterial Efficiency

Observing the obtained images by CLSM, the interaction between the BSA-Tpy NPs and bacteria could be visualized to some extent. Gram-positive MRSA and Gram-negative *E. coli*, two kinds of typical pathogenic bacteria, were selected as the evaluation of imaged fluorescence in our experiment. The concentration of BSA-Tpy was 50 $\mu\text{g/mL}$ according to the cytotoxicity test. General photosensitizers only have the ability to select Gram-positive bacteria to achieve imaging function, and the literature reports that significant structural differences may explain this. It has been demonstrated that both the enveloped Gram-positive and Gram-negative bacteria of the cells are negatively charged, which facilitates the adsorption of positively charged photosensitizers therewith. However, the difference between Gram-negative bacteria, Gram-positive bacteria is that the later one has only a single lipid membrane covered with a thick layer of cross-linked peptidoglycan shell structure. As shown in Figure 4A, we found that the red fluorescence at pH 5.0, there were clear fluorescence signal in bacteria including Gram-negative *E. coli*. The result was attributed to the structure of the bacteria and the response of the material in different environments. Amounts of gram-negative bacteria can also be stained by photosensitizers after modification of our nanocarriers. Hence, the problem was solved according to designed strategy that most photosensitizers can only act on the Gram-positive bacteria. Besides, it was can be seen that the bacteria were detected by clear red light, which also proved the superiority of our materials possessing broad absorption, long emission wavelengths and excellent AIE property.

We evaluated the photodynamic antibacterial effect by using plate counting method. *E. coli* and MRSA without BSA-Tpy NPs and white light were set as control groups. The selected experimental concentration was based on the cytotoxicity test and bacterial staining performance. Gram-negative *E. coli* and Gram-positive MRSA were set as control groups without BSA-Tpy without white light. It is shown in Figure 4B, the control group almost did not change on the agar plates. Both MRSA and *E. coli* with BSA-Tpy for 25 min continuous white light irradiation in an acidic environment were killed totally with a colony forming unit (CFU) reduction rate about 100%. This is because the

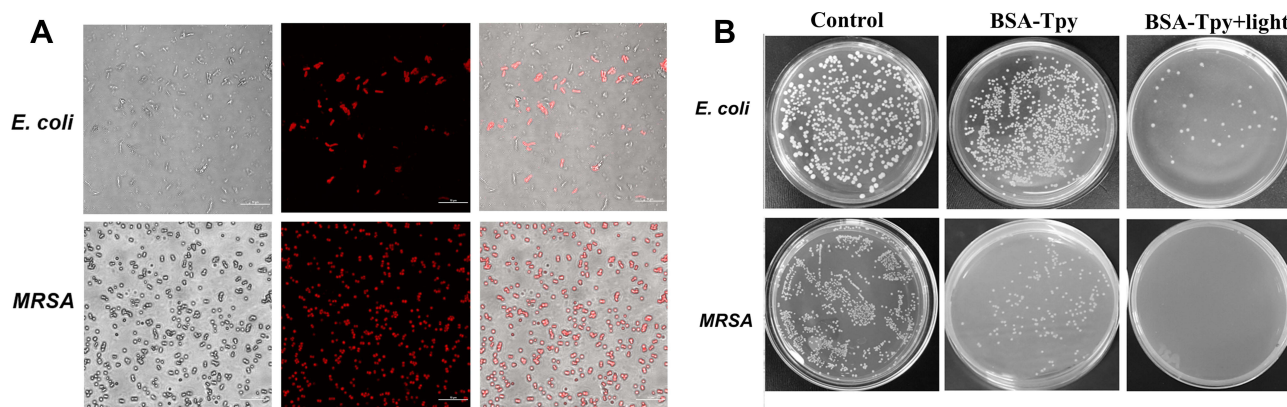


Figure 4 (A) Bright-field and fluorescent images of bacteria. *E. coli*, MRSA and were incubated with BSA-Tpy at pH 5.0 and for 25 min before imaging (Scale bar: 10 μm). **(B)** Image of plate counting method for *E. coli* and MRSA with of BSA-Tpy at pH 5.0.

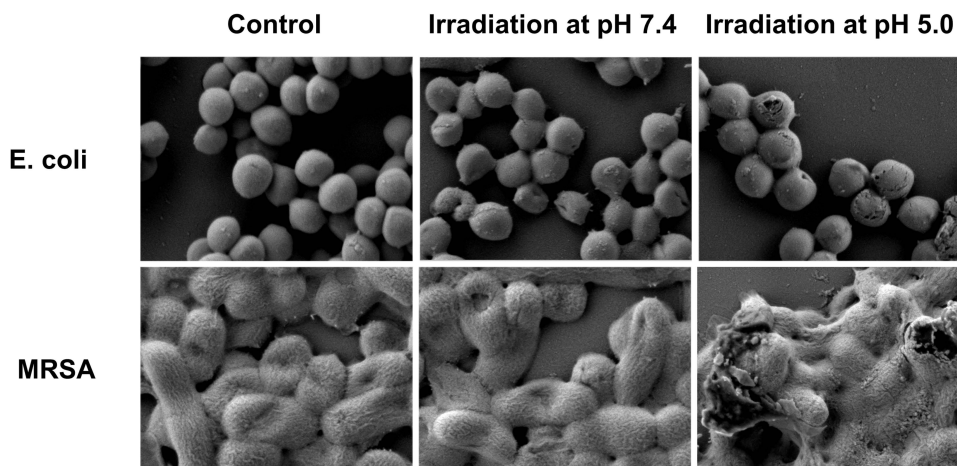


Figure 5 Visualizing BSA-Tpy NPs-induced morphological changes of bacteria, MRSA and *E. coli* for 25 min white light irradiation were imaged by SEM at pH 7.4 and pH 5.0 respectively, bacteria without treatment were set as controls.

ROS generation of antimicrobial platform of BSA-Tpy NPs could physically destroy the integrity of bacterial structure, resulting in the leakage of intracellular components due to the composition of quaternary ammonium salt, furtherly enhancing the photodynamic bacteria invasion under white light irradiation. At the acidic environment, the protonation of the material increased the positively charge of BSA-Tpy NPs and finally contributed to the charge-mediated targeting bacteria to enhance the antibacterial efficiency. The ROS generation mechanism of PDAT is complicated and mentioned above, some other studies have explained that PDAT induced oxidative stress, reduced DNA replication, and synthesis of proteins, indicating that the antimicrobial agent had antioxidant stress on pathogenic bacteria.³³

Additionally, to get more insights into the interaction between the BSA-Tpy NPs and bacteria SEM analysis were employed to detect the morphological changes of bacteria under white light irradiation. As is shown in Figure 5, without light irradiation and BSA-Tpy NPs treatment, the morphologies of the MRSA and *E. coli* showed usual shapes with clear borders and cell walls. Besides, with the BSA-Tpy NPs and light treatment, the damage and deformation were observed only in Gram-positive bacteria MRSA at pH 7.4; however, when pH reached to 5.0, all bacteria including *E. coli* were damaged. We could conclude that under acidic conditions, the material and bacteria could better combine with each other by the electrostatic interaction forces. This is consistent with the results of the tests mentioned above. The results of SEM are consistent with those of the plate counting method, which further proved that the material has good antibacterial properties against both gram-positive and gram-negative bacteria under both acidic and light conditions.

Evaluation on Rat Wound Models

For further studying the effect toward wound healing of the material in vivo, the therapeutic effect of the material on bacterial infection wound in rats was tested. As depicted in Figure 6A, we established an animal model of wound infection with MRSA on the dorsal skin of Wistar rats. At different points in time, the pictures of the wound were taken for each to see how the bacterial infection was recovering. After 7 days, the area of MRSA-infected wounds became more severe without any treatment or only BSA-Tpy without light treatment. However, in the presence of both the BSA-Tpy and white light treatment significantly reduced the wound area indicating that the material could effectively inhibit the wound bacterial infection under light irradiation (Figure 6B). Due to the large amount of ROS produced by the BSA-Tpy under light irradiation cause the death of MRSA, decreasing the degree of infection. The results above indicated the effect of promoting wound healing of BSA-Tpy. Next, we further tested the biocompatibility in vivo using wound-healing rats. As shown in Figure 6C, the material was not found to be toxic to rats by H&E staining of organs, proving good biocompatibility.

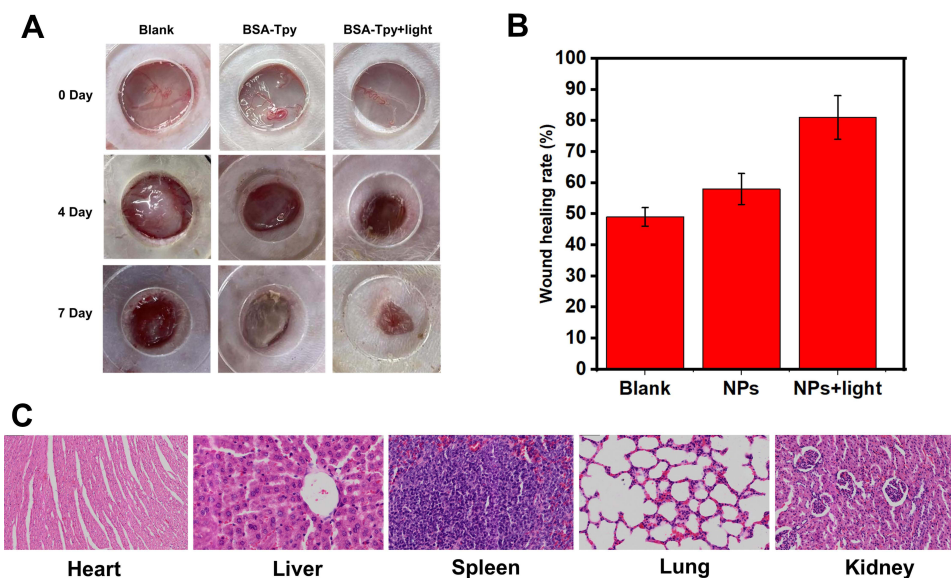


Figure 6 The evaluation of BSA-TpyNPs in treatment of bacteria-infected wounds of rats in vivo. **(A)** Images of MRSA-infected wounds after dealing with NPs with/without light ($50 \text{ mW} \cdot \text{cm}^{-2}$) on day 0 and day 4 postinfection. **(B)** The wounding healing rate of the MRSA-infected wound area on day 4 after the injury. **(C)** H&E staining of the organs in rats after treatment for 4 days.

Conclusion

In summary, we have developed a feasible method for photodynamic antibacterial therapy, possessing excellent biocompatibility and high antibacterial efficiency with good fluorescence imaging property. The results confirmed that such BSA-Tpy NPs delivery systems could maintain stability in a neutral environment enhanced targeting ability to the bacteria in the acidic environment due to the change in surface potential. Under the irradiation of white light, the photosensitizer will produce reactive oxygen species, destroy the structure of bacteria, and further induce bacteria to produce reactive oxygen species. Therefore, both exogenous and endogenous ROS can be generated simultaneously, greatly improving the antibacterial efficiency. This engineered material can combat both Gram-positive and Gram-negative bacterial infections greatly improving the antibacterial efficiency under light irradiation. What is more, this method may have potential application prospect that could expand to photodynamic anti-cancer therapy as well. Considering all the great significance above, we will continue to search for the possibilities in the following exploration.

Ethical Statement

All animal experimentations were approved by the Institutional Animal Care and Ethics Committee of the affiliated Nanhua hospital, University of south China (Hengyang, China) and performed in accordance with the principles and procedures of the National Institutes of Health (NIH) Guide for the Care and Use of Laboratory Animals and the Guidelines for Animal Treatment of University of south China.

Funding

This work was funded by the Hunan Provincial Science and Technology Department (2021SK4030), Major Special Project of Hunan Provincial Health and Family Planning Commission (20201906), Education Department of Hunan Province (21C0277), Hengyang Science and Technology Department (2021115).

Disclosure

The authors report no conflicts of interest in this work.

References

1. Zeng Q, Qi X, Shi G, et al. Wound dressing: from nanomaterials to diagnostic dressings and healing evaluations. *ACS Nano*. 2022;16(2):1708–1733. doi:10.1021/acsnano.1c08411
2. Wang S, Zhou Y, Liang X, et al. Platinum-cerium bimetallic nano-raspberry for atherosclerosis treatment via synergistic foam cell inhibition and P2Y12 targeted antiplatelet aggregation. *Chem Eng J*. 2022;430:132859. doi:10.1016/j.cej.2021.132859
3. Songca SP, Adjei Y. Applications of antimicrobial photodynamic therapy against bacterial biofilms. *Int J Mol Sci*. 2022;23(6):3209. doi:10.3390/ijms23063209
4. Polat E, Kang K. Natural photosensitizers in antimicrobial photodynamic therapy. *Biomedicines*. 2021;9(6):584. doi:10.3390/biomedicines9060584
5. Masiera N, Bojarska A, Gawryszewska I, et al. Antimicrobial photodynamic therapy by means of porphyrine photosensitizers. *J Photochem Photobiol B*. 2017;174:84–89. doi:10.1016/j.jphotobiol.2017.07.016
6. Wang Y, Xu Y, Guo X, et al. Enhanced antimicrobial activity through the combination of antimicrobial photodynamic therapy and low-frequency ultrasonic irradiation. *Adv Drug Deliv Rev*. 2022;183:114168. doi:10.1016/j.addr.2022.114168
7. Awad M, Thomas N, Barnes TJ, et al. Nanomaterials enabling clinical translation of antimicrobial photodynamic therapy. *J Control Release*. 2022;346:300–316. doi:10.1016/j.jconrel.2022.04.035
8. Agazzi ML, Ballatore MB, Durantini AM, et al. BODIPYs in antitumoral and antimicrobial photodynamic therapy: an integrating review. *J Photochem Photobiol C*. 2019;40:21–48. doi:10.1016/j.jphotochem.2019.04.001
9. Zhang Y, Zhou K, Jiang H, et al. Poly (NIPAM-co-thienoviologen) for multi-responsive smart windows and thermo-controlled photodynamic antimicrobial therapy. *J Mater Chem A*. 2021;9:18369–18376. doi:10.1039/D1TA03936A
10. Dias LD, Blanco KC, Mfouo-Tynga IS, et al. Curcumin as a photosensitizer: from molecular structure to recent advances in antimicrobial photodynamic therapy. *J Photochem Photobiol C*. 2020;45:100384.
11. Wang K-N, Liu L-Y, Mao D, et al. A nuclear-targeted AIE photosensitizer for enzyme inhibition and photosensitization in cancer cell ablation. *Angew Chem Int Ed Engl*. 2022;61(15):e202114600. doi:10.1002/anie.202114600
12. Tavakkoli Yarak M, Pan Y, Hu F, et al. Nanosilver-enhanced AIE photosensitizer for simultaneous bioimaging and photodynamic therapy. *Mater Chem Front*. 2020;4(10):3074–3085. doi:10.1039/D0QM00469C
13. He X, Situ B, Gao M, et al. Stereotactic photodynamic therapy using a two-photon AIE photosensitizer. *Small*. 2019;15(50):1905080. doi:10.1002/sml.201905080
14. Chen C, Ni X, Tian H-W, et al. Calixarene-based supramolecular AIE dots with highly inhibited nonradiative decay and intersystem crossing for ultrasensitive fluorescence image-guided cancer surgery. *Angew Chem Int Ed Engl*. 2020;59(25):10008–10012. doi:10.1002/anie.201916430
15. Zhao W, He Z, Peng Q, et al. Highly sensitive switching of solid-state luminescence by controlling intersystem crossing. *Nat Commun*. 2018;9(1):3044. doi:10.1038/s41467-018-05476-y
16. Yang L, Wang X, Zhang G, et al. Aggregation-induced intersystem crossing: a novel strategy for efficient molecular phosphorescence. *Nanoscale*. 2016;8(40):17422–17426. doi:10.1039/C6NR03656B
17. Yang Y, Tian -J-J, Wang L, et al. D- π -A type carbazole and triphenylamine derivatives with different π -conjugated units: tunable aggregation-induced emission (AIE) and mechanofluorochromic properties. *J Photochem Photobiol A*. 2022;429:113905. doi:10.1016/j.jphotochem.2022.113905
18. Kathirvelan D, Mayakrishnan S, Uma Maheswari N, et al. A simple D- π -A system of phenanthroimidazole- π -fluorenone for highly efficient non-doped bipolar AIE luminogens: synthesis, and molecular optical, thermal and electrochemical properties. *New J Chem*. 2020;44(5):1785–1794. doi:10.1039/C9NJ05226G
19. Wang L, Xia Q, Zhang Z, et al. Precise design and synthesis of an AIE fluorophore with near-infrared emission for cellular bioimaging. *Mater Sci Eng C*. 2018;93:399–406. doi:10.1016/j.msec.2018.08.012
20. Gao C, Hossain MK, Wahab MA, et al. Understanding the details of aggregation-induced emission (AIE) effect in D- π -A type imidazolium-based compounds through the stepwise change of rotatable moieties. *Dyes Pigm*. 2018;160:909–914. doi:10.1016/j.dyepig.2018.08.032
21. Luo W, Tan Y, Gui Y, et al. Near-infrared-emissive AIE bioconjugates: recent advances and perspectives. *Molecules*. 2022;27(12):3914. doi:10.3390/molecules27123914
22. Xu L, Zhang S, Liang X, et al. Novel biocompatible AIEgen from natural resources: palmatine and its bioimaging application. *Dyes Pigm*. 2020;184:108860. doi:10.1016/j.dyepig.2020.108860
23. Van Lysebetten D, Malfanti A, Deswarte K, et al. Lipid-polyglutamate nanoparticle vaccine platform. *ACS Appl Mater Interface*. 2021;13(5):6011–6022. doi:10.1021/acsmi.0c20607
24. Thorp EB, Boada C, Jarbath C, et al. Nanoparticle platforms for antigen-specific immune tolerance. *Front Immunol*. 2020;11:945. doi:10.3389/fimmu.2020.00945
25. Ortelli S, Costa AL, Zanoni I, et al. TiO₂@BSA nano-composites investigated through orthogonal multi-techniques characterization platform. *Colloids Surf B Biointerfaces*. 2021;207:112037. doi:10.1016/j.colsurfb.2021.112037
26. Shahgholian N, Rajabzadeh G. Preparation of BSA nanoparticles and its binary compounds via ultrasonic piezoelectric oscillator for curcumin encapsulation. *J Drug Deliv Sci Technol*. 2019;54:101323. doi:10.1016/j.jddst.2019.101323
27. Zhang W, Jiang P, Chen Y, et al. Suppressing the cytotoxicity of CuO nanoparticles by uptake of curcumin/BSA particles. *Nanoscale*. 2016;8(18):9572–9582. doi:10.1039/C6NR02181F
28. Chern C-S, Lee C-K, Kuan C, et al. Adsorption of BSA on the amphiphilic PEG graft copolymer-coated particles. *Colloid Polym Sci*. 2005;283(8):917–924. doi:10.1007/s00396-004-1241-x
29. Wang Y, Wu Y, Liu Y, et al. BSA-mediated synthesis of bismuth sulfide nanotheranostic agents for tumor multimodal imaging and thermoradiotherapy. *Adv Funct Mater*. 2016;26(29):5335–5344. doi:10.1002/adfm.201601341
30. Jeon S, Oberreit DR, Van Schooneveld G, et al. Ion-mobility-based quantification of surface-coating-dependent binding of serum albumin to superparamagnetic iron oxide nanoparticles. *ACS Appl Mater Interfaces*. 2016;8(37):24482–24490. doi:10.1021/acsmi.6b09070
31. Zhang CY, Dong X, Gao J, et al. Nanoparticle-induced neutrophil apoptosis increases survival in sepsis and alleviates neurological damage in stroke. *Sci Adv*. 2019;5(11):eaax7964. doi:10.1126/sciadv.aax7964

32. Kang M, Zhou C, Wu S, et al. Evaluation of structure-function relationships of aggregation-induced emission luminogens for simultaneous dual applications of specific discrimination and efficient photodynamic killing of gram-positive bacteria. *J Am Chem Soc.* 2019;141(42):16781–16789. doi:10.1021/jacs.9b07162
33. Ren B, Li K, Liu Z, et al. White light-triggered zwitterionic polymer nanoparticles based on an AIE-active photosensitizer for photodynamic antimicrobial therapy. *J Mater Chem B.* 2020;8(47):10754–10763. doi:10.1039/D0TB02272A

Infection and Drug Resistance

Dovepress

Publish your work in this journal

Infection and Drug Resistance is an international, peer-reviewed open-access journal that focuses on the optimal treatment of infection (bacterial, fungal and viral) and the development and institution of preventive strategies to minimize the development and spread of resistance. The journal is specifically concerned with the epidemiology of antibiotic resistance and the mechanisms of resistance development and diffusion in both hospitals and the community. The manuscript management system is completely online and includes a very quick and fair peer-review system, which is all easy to use. Visit <http://www.dovepress.com/testimonials.php> to read real quotes from published authors.

Submit your manuscript here: <https://www.dovepress.com/infection-and-drug-resistance-journal>